Journal of Solid State Chemistry 182 (2009) 1291–1296

Contents lists available at ScienceDirect

Journal of Solid State Chemistry

journal homepage: www.elsevier.com/locate/jssc

Nanoscale formation of new solid-state compounds by topochemical effects: The interfacial reactions ZnO with Al_2O_3 as a model system

Sonia Pin [a], Paolo Ghigna [a,*], Giorgio Spinolo [a], Eliana Quartarone [a], Piercarlo Mustarelli [a], Francesco D'Acapito [b], Andrea Migliori [c], Gianluca Calestani [d]

[a] INSTM, IENI/CNR, Dipartimento di Chimica Fisica "M. Rolla", Università di Pavia, Viale Taramelli 16, I-27100 Pavia, Italy
[b] CNR-INFM-OGG c/o ESRF, GILDA CRG, 6, Rue Jules Horowitz, F-38043 Grenoble, France
[c] LAMEL/CNR, I 40129 Bologna, Italy
[d] Dipartimento di Chimica Generale ed Inorganica, Chimica Analitica, Chimica Fisica, Parco Area delle Scienze 17, 43100 Parma, Italy

ARTICLE INFO

Article history:
Received 3 November 2008
Received in revised form
18 February 2009
Accepted 25 February 2009
Available online 5 March 2009

Keywords:
Topochemistry
XAS
Reactivity in the solid state

ABSTRACT

The chemical reactivity of thin layers (ca. 10 nm thick) of ZnO deposited onto differently oriented Al_2O_3 single crystals has been investigated by means of atomic force microscopy inspections and X-ray absorption spectroscopy at the Zn–K edge. The $(0001)_{ZnO}\|(11\bar{2}0)_{sapphire}$ interface yields the $ZnAl_2O_4$ spinel and a quite stable film morphology. Instead, the $(11\bar{2}0)_{ZnO}\|(1\bar{1}02)_{sapphire}$ and $(0001)_{ZnO}\|(0001)_{sapphire}$ interfaces give origin to a new compound (or, possibly, even two new compounds), whose chemical nature is most likely that of a ZnO/Al_2O_3 phase, with still unknown composition and crystal structure. In addition, in the last two cases, films collapse into prismatic twins of ca. 1 μm in dimension. These experimental findings demonstrate that in a solid-state reaction, the topotactical relationships between the reacting solids are of crucial importance not only in determining the kinetic and mechanisms of the process in its early stages, but even the chemical nature of the product.

1. Introduction

Solid-state reactions are of extreme interest both for technological applications and from the point of view of basic science. In fact, on the one hand, many important materials are currently prepared by solid-state synthesis (almost all ceramics materials, for instance); on the other hand, for example, reactions in the solid state occur in many geological processes such as mineral metamorphism.

The kinetics and mechanisms of these reactions are typically studied making use of mono-dimensional chemical diffusion experiments. In such an experiment, two single crystals (or well-sintered pellets) of the reacting solids are kept in contact at high temperature and the thickness of the product layer that forms in between is measured as a function of time. When the layer thickness exceeds a certain value (usually $>1\,\mu m$) the growth of the product layer is driven by the diffusion of some constituents inside the product layer itself. The theory underlying these experiments (see [1]) assumes that local chemical equilibrium is attained in this regime at both interfaces (between each reagent phase and the product phase), and shows that the layer thickness increases with the square root of time (parabolic growth law): the excellent agreement between the rate constant so measured and independently obtained diffusion coefficient data then gives a trustworthy assessment of the reaction mechanism in this long reaction time regime.

However, very little (if nothing at all) is known about the very early stages of this kind of processes, when local chemical equilibrium is not yet attained at the interfaces and the chemical kinetics is not driven by long range diffusion, but by the motion of the interfaces [1]. Also, the mechanisms and the kinetics of the interfacial reactions (that are, in a sense, the 'true' chemical reactions) are completely unknown. This is largely due to the lack of an experimental probe and of an established procedure for studying such aspects. It is quite straightforward to foresee that, in the regime of interfacial driven kinetics, the topotactical relationships between the reacting interfaces can be of extreme relevance.

In a recent paper it has been shown that some insight into the mechanisms and the kinetics of solid-state reactions in the early stages can be obtained by: (i) performing the reaction using at least one of the reactants in form of a very thin film (of the order of 10 nm), (ii) using a local probe for the local chemical environment of one of the constituents such as X-ray absorption spectroscopy (XAS) [2,3].

In these previous works, the reaction $NiO+Al_2O_3 \rightarrow NiAl_2O_4$ has been studied. Aim of the present work is to study the early stage

* Corresponding author. Fax: +39 00382 987575.
E-mail address: paolo.ghigna@unipv.it (P. Ghigna).

0022-4596/$ - see front matter © 2009 Elsevier Inc. All rights reserved.
doi:10.1016/j.jssc.2009.02.027

reactivity between ZnO and Al_2O_3. This system has been chosen as: (i) $ZnAl_2O_4$ is a direct spinel, (ii) only this compound exists in the equilibrium ZnO/Al_2O_3 phase diagram [4], (iii) in the ZnO/Al_2O_3 system, the oxygen sublattice has to rearrange from a hexagonal-close-packed (hcp) to a face-centered-cubic (fcc) arrangement at both reaction fronts: on the contrary in the NiO/Al_2O_3 system, the rearrangement of the oxygen sublattice occurs only at a single interface (spinel/sapphire), (iv) a quite large number of topotactical relationships can be found in the literature for the interface between the wurtzite ZnO structure and the Al_2O_3 sapphire structure [5,6 and references therein], and (v) there are a number of technological applications, ranging from catalysis to optoelectronics to spintronics [7–10] for which ZnO thin films deposited onto Al_2O_3 are used or studied as promising systems.

Here, the reactivity between a thin ZnO film and different Al_2O_3 surfaces has been studied by means of XAS; atomic force microscopy (AFM) has been used as a supporting technique in order to monitor the morphology of the films during the reactions. This work should also be intended as the first part of a more complete investigation aiming at shading light onto the more general problem of the mechanisms of the initial stages of solid-state reactions.

2. Experimental

A 10 nm thick ZnO thin films have been obtained [11] by RF-magnetron sputtering of ZnO (Aldrich, 99.99%) onto Al_2O_3 $(1\bar{1}02)$, $(11\bar{2}0)$, and (0001) oriented single crystals (MaTecK) at room temperature. After the deposition the films have been treated at 600 °C for 20 min. This is the minimum temperature required for obtaining well crystalline and well oriented films on all the investigated surfaces: indeed, the as grown film on the sapphire $(1\bar{1}02)$ surface, is randomly oriented (as shown by the X-ray absorption near edge structure (XANES) dichroic spectra, see below), and for example a treatment at 300 °C does not permit to obtain an oriented film and therefore a clear topotactic relationship. Subsequently, a treatment at 800 °C for 120 min has been performed, to allow the interfacial reactions to take place: this temperature has been used because is large enough to permit chemical reactivity but not ZnO evaporation, that was observed at higher temperatures. All the treatments have been done in air. The mean surface roughness of the films after the treatment at 600 °C is 7 nm.

Fluorescence X-ray absorption fine structure (XAFS) data were collected at GILDA beamline [12] (European Synchrotron Radiation Facility, ESRF, Grenoble) at the Zn–K edge. A Si (311) double crystal monochromator was used; the harmonic rejection was realized by Pd mirrors, having a cut-off energy of 20 keV. A 13-elements high purity germanium detector was used for the collection of the fluorescence spectra, with the samples at 14.5° (84.5°) with respect to the incoming beam (that is with the radiation electric field parallel (perpendicular) PAR (PER) to the sample surface, orientation). Unpolarized spectra have been obtained by averaging the spectra taken with the two different polarizations. The measurements were performed at room temperature. To obtain a reasonable signal to noise ratio, the integration time was adjusted to give $\cong 10^6$ counts in the fluorescence channel; in addition, in order to avoid distortions of the spectra, the count rate of each element was kept well below the saturation limit. For the XANES analysis the spectra were processed by subtracting the smooth pre-edge background fitted with a straight line. Each spectrum was then normalized to unit absorption at 800 eV above the edge, where the extended X-ray absorption fine structure (EXAFS) oscillations were not visible any more. The EXAFS fitting has been performed by means of the FEFF8 code [13]. The goodness of fit (GOF) is given by the *R-factor* parameter which is scaled to the magnitude of the data itself

$$R = \frac{\sum_{i=1}^{N}\{[\mathrm{Re}(f_i)]^2 + [\mathrm{Im}(f_i)]^2\}}{\sum_{i=1}^{N}\{[\mathrm{Re}(\chi_{data})]^2 + [\mathrm{Im}(\chi_{data})]^2\}}$$

This number gives a sum-of-squares measure of the fractional misfit. For good fits to carefully measured data on concentrated samples, $R \leqslant 0.02$. The accuracy of amplitude and phase-shifts calculated by the program have been checked by fitting the spectrum of powdered ZnO, and comparing the fitted radial distances with crystallographic values, that have been recovered with an accuracy better than 0.01 Å.

AFM images were collected with an Autoprobe CP Research scanning probe microscopy (SPM, VEECO), operating in contact mode, by means of sharpened pyramidal silicon tips (curvature radius <20 nm) onto V-shaped cantilevers (resonant frequency, 120 kHz; force constant, 0.5 N/m). For each analysed sample, scans of different areas were carried out with a resolution of 512 pixels and a scan rate ranging between 1.0 and 1.5 Hz. A standard second-order flattening processing of the images was performed in order to correct the scanner nonlinearity.

Preliminary transmission electron microscopy (TEM) investigations were performed on the samples using an FEI Tecnai F20 apparatus operating at 200 kV. The specimens were cooled by a temperature controlled LN holder. Scanning transmission electron microscopy (STEM) images were recorded using a high angle dark field detector.

3. Results and discussion

Fig. 1 shows, as an example, the raw fluorescence data at the Zn–K edge for a ZnO film deposited onto a $(1\bar{1}02)$ Al_2O_3 single crystal and heated at 600 °C for 20 min: for this spectrum the electrical field vector is perpendicular to the sample surface. The statistical noise was estimated by fitting the spectrum after 10 400 eV, i.e. where the EXAFS oscillations are no longer visible, with a straight line. After normalization for the edge jump the noise was estimated to be 10^{-3}: this figure is representative of the quality of all the collected spectra. Given that the samples are challenging, this value for the noise should be regarded as very good.

Fig. 2 shows the linear dichroism for the Zn–K edge XANES for the sample of Fig. 1: a huge dichroic effect is well apparent. Comparison with literature data at the Zn–K edge for a wurtzite single crystal and films [14,15] shows that the ZnO film is highly oriented, if not single crystal. In particular, it should be noted that our XANES manifold for the PAR(PER) orientation corresponds to

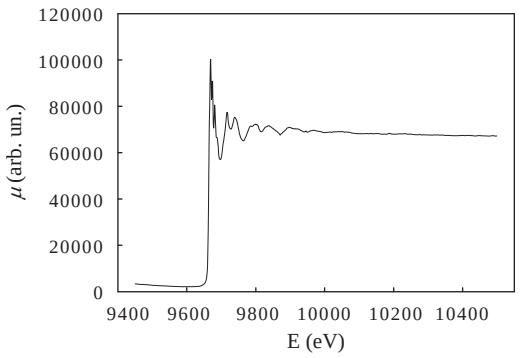

Fig. 1. Raw fluorescence data at the Zn–K edge for a ZnO film deposited onto a $(1\bar{1}02)$ Al_2O_3 single crystal and heated at 600 °C for 20 min (PAR orientation).

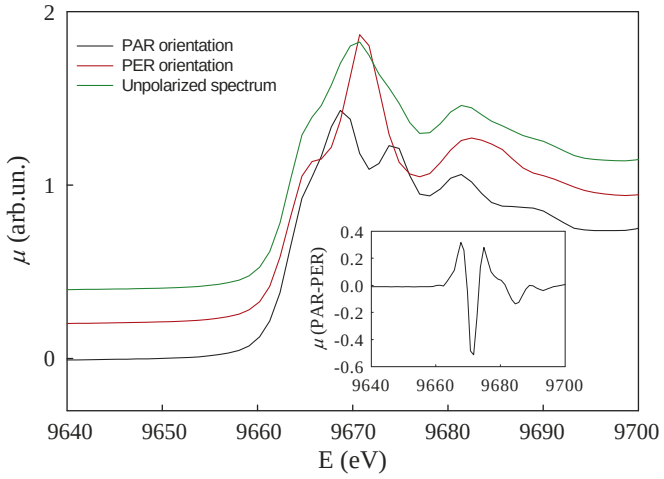

Fig. 2. Linear dichroism for the sample of Fig. 1. In this figure the XANES spectra are shown, collected with the two different orientations of the electric field with respect to the sample surface, as described in the text. The unpolarized spectrum, obtained as described in the experimental section, is also shown for reference. In this and following figures, the spectra have been shifted along the *y* axis for convenience. The inset shows the linear dichroism, defined as the difference between the spectrum collected with the electric field parallel and perpendicular (PAR–PER) to the sample surface.

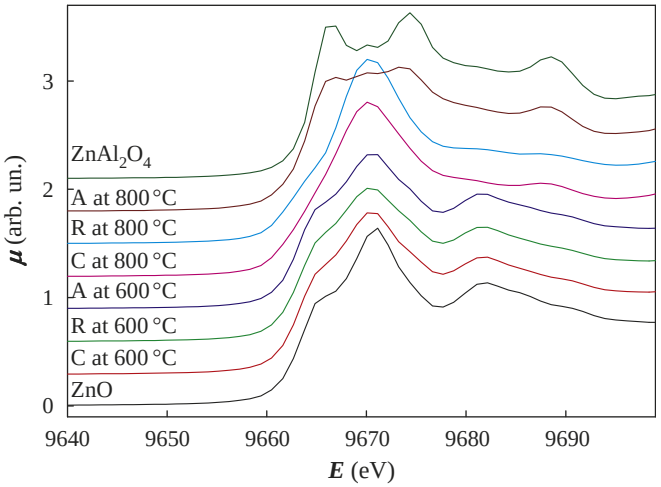

Fig. 3. Unpolarized Zn–K edge XANES spectra of the samples investigated in this work. A: $(0001)_{ZnO}\|(11\bar{2}0)_{sapphire}$; C: $(0001)_{ZnO}\|(0001)_{sapphire}$; R: $(11\bar{2}0)_{ZnO}\|(1\bar{1}02)_{sapphire}$. For reference, also the XANES of powdered ZnO and $ZnAl_2O_4$ are shown.

that of a highly oriented wurtzite film [15] with the *c* axis *perpendicular* to the film surface for the PER(PAR) orientation: therefore in our case the *c* axis is *parallel* to the film surface . The topotactic relationship between the ZnO film and sapphire is $(11\bar{2}0)_{ZnO}\|(1\bar{1}02)_{sapphire}$ and $[0001]_{ZnO}\|(1\bar{1}01)_{sapphire}$, as already observed by Lim et al. [5] and Ay et al. [6]. The same comparison shows that the film deposited onto the $(11\bar{2}0)$ and (0001) Al_2O_3 single crystals is found with the *c* axis of wurtzite *perpendicular* to the film surface. The topotactic relationships between ZnO film and sapphire are therefore $(0001)_{ZnO}\|(11\bar{2}0)_{sapphire}$, and $(0001)_{ZnO}\|(0001)_{sapphire}$, again in agreement with previous works [5,6].

The different reactions of the different films are made apparent by looking at Figs. 3 and 4. In particular in Figs. 3 and 4 the Zn–K edge unpolarized XANES and EXAFS (with the corresponding FT) spectra for the reacted films after the thermal treatments described in the experimental, respectively, are shown. For comparison, in these figures the spectra of powdered ZnO and $ZnAl_2O_4$ are also shown. In addition, for the sake of better clarity, in these figures the $(0001)_{ZnO}\|(11\bar{2}0)_{sapphire}$, $(0001)_{ZnO}\|(0001)_{sapphire}$ and $(11\bar{2}0)_{ZnO}\|(1\bar{1}02)_{sapphire}$ are labelled A, C and R, respectively, according to the common nomenclature for the sapphire surfaces.

At 600 °C it is seen at a glance that all the films have the same XANES and EXAFS spectra, and that these spectra correspond very nicely to the one of powdered ZnO.

When the samples are treated at 800 °C, impressive changes are found in the spectra.

In details, for the film deposited onto the $(11\bar{2}0)$ Al_2O_3 single crystal, at 800 °C the Zn–K edge XANES manifold changes from a ZnO-like structure to a $ZnAl_2O_4$-like structure. Therefore, for the $(0001)_{ZnO}\|(11\bar{2}0)_{sapphire}$ interface, the $ZnO+Al_2O_3 \rightarrow ZnAl_2O_4$ reaction takes place at 800 °C.

On the contrary, for the $(11\bar{2}0)_{ZnO}\|(1\bar{1}02)_{sapphire}$ and $(0001)_{ZnO}\|(0001)_{sapphire}$ interfaces, a well different behaviour is found: in particular, in both these cases, the spectral features at 9665 and 9683 eV are strongly depressed when compared to those of ZnO; in addition, these two interfaces show a very similar behavior. The scenario is here quite intriguing, as demonstrated by the Zn–K edge EXAFS spectra displayed in Fig. 4. Inspecting in particular at

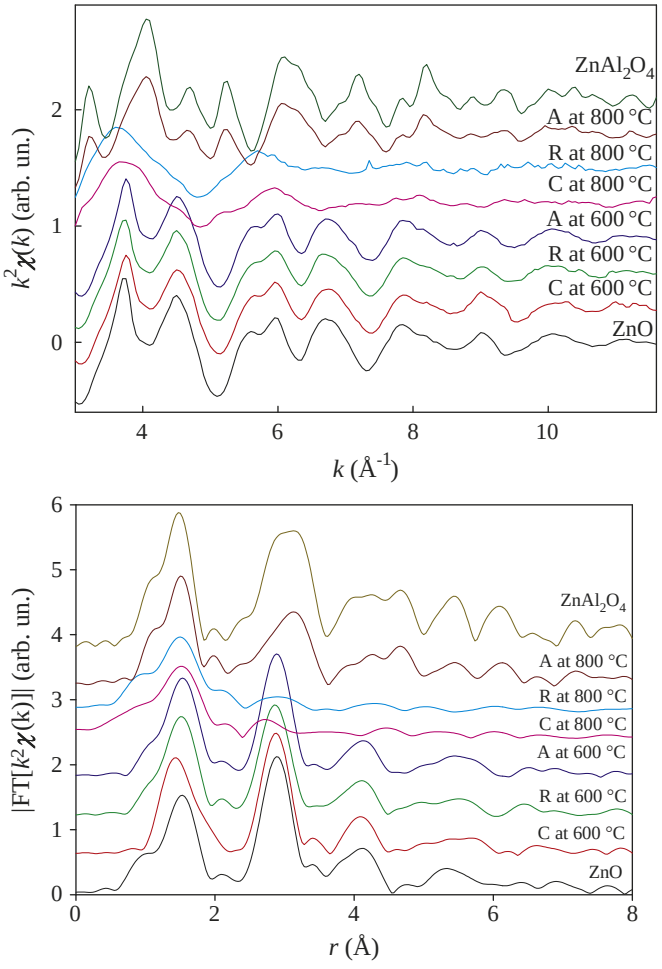

Fig. 4. Unpolarized Zn–K edge EXAFS spectra (upper panel) and EXAFS Fourier transform (lower panel) of the samples investigated in this work. The spectra of powdered ZnO and $ZnAl_2O_4$ are also shown for reference. For the labelling in this figure see caption of Fig. 3.

the first peak of the EXAFS FT, which is due to the nearest neighbours (NN), it is quite apparent that the Zn–O first coordination shell remains almost unchanged, while the peak

corresponding to the next nearest neighbours (NNN) becomes strongly depressed after firing at 800 °C. Therefore, during the process, the NN coordination of Zn remains tetrahedral as in the ZnO wurtzite-type structure, but with a considerable amount of static disorder in the NNN shell.

Additional structural information can be obtained by the EXAFS fitting. The fitting procedure adopted here started from the above consideration about the NN and NNN shells: therefore, the fits have been made by using a wurtzite-like structural model, and, to account for the static disorder in the NNN shell, by substituting some of the Zn atoms in this shell with Al, for a total of 12 atoms in the wurtzite structure. In Fig. 5 the best fit is shown for $(0001)_{ZnO}\|(0001)_{sapphire}$ interface and the results are summarized in Table 1. The best agreement is obtained if one third of the Zn atoms is substituted by Al in the NNN shell of Zn (model 5 of Table 1). In fact, in this last case the GOF (as given by the *R*-factor as defined in the experimental) shows the best figure; in addition the bond valence sum (BVS) [16] for Zn converges to more sensible values by increasing the amount of Al in the NNN shell, up to a Zn/Al atomic ratio close to 1/3. It should be noted that, even in this case, the disorder is quite important, as indicated by the very high value for the σ^2 parameter. Additionally, it is worth noting that other models have been tested with more Al in the NNN shell: the result is a drastic worsening of the GOF.

Somewhat different results are obtained if the same fitting procedure is applied to the $(11\bar{2}0)_{ZnO}\|(1\bar{1}02)_{sapphire}$ interface (see Table 2 and Fig. 6). In this case, while the introduction of some Al results in a improved GOF, the trend is not monotonous and sensible values for the BVS are obtained only when one half of the Zn atoms in the NNN shell are replaced by Al (model 4). It should be noticed that this model, even as is not the one that gives the most favorable GOF, should be considered as the most consistent, as it gives the most reasonable figures for the BVS and errors in the fitting parameters.

It may be worth noticing that the fits displayed in Figs. 5 and 6 *do not* account for all the features of the EXAFS spectra.

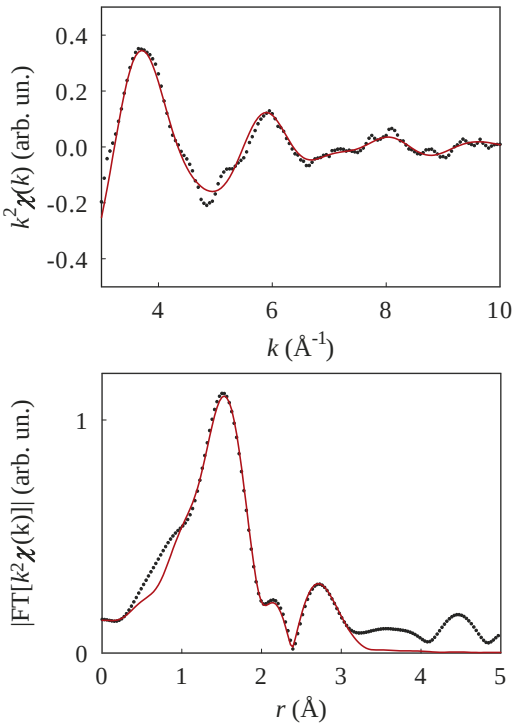

Fig. 5. EXAFS fitting results for the $(0001)_{ZnO}\|(0001)_{sapphire}$ interface at 800 °C, according to model 5 of Table 1 (dots: experimental; line: predicted).

Table 1
EXAFS fitting parameters for the spectrum of Fig. 5, with different structural models.

$(0001)_{ZnO}\|(0001)_{sapphire}$, model 1				
NN shell				
Atom	*n*	*r*	σ^2/*BVS*	*R*
O	1	2.0 (1)	0.01 (6)/1.76	0.021
O	3	2.0 (6)		
NNN shell				
Atom	*n*	*r*	σ^2	
Zn	12	3.37 (1)	0.03 (1)	
Al	0	–		
$(0001)_{ZnO}\|(0001)_{sapphire}$, model 2				
NN shell				
Atom	*n*	*r*	σ^2/*BVS*	*R*
O	1	1.89 (6)	0.005 (6)/1.84	0.011
O	3	2.03 (1)		
NNN shell				
Atom	*n*	*r*	σ^2	
Zn	11	3.11 (3)	0.033 (8)	
Al	1	3.5 (1)		
$(0001)_{ZnO}\|(0001)_{sapphire}$, model 3				
NN shell				
Atom	*n*	*r*	σ^2/*BVS*	*R*
O	1	1.88 (5)	0.005 (5)/1.86	0.010
O	3	2.03 (1)		
NNN shell				
Atom	*n*	*r*	σ^2	
Zn	10	3.11 (3)	0.031 (7)	
Al	2	3.16 (9)		
$(0001)_{ZnO}\|(0001)_{sapphire}$, model 4				
NN shell				
Atom	*n*	*r*	σ^2/*BVS*	*R*
O	1	1.85 (3)	0.005 (3)/1.99	0.007
O	3	2.01 (1)		
NNN shell				
Atom	*n*	*r*	σ^2	
Zn	9	3.10 (2)	0.027 (5)	
Al	3	3.15 (5)		
$(0001)_{ZnO}\|(0001)_{sapphire}$, model 5				
NN shell				
Atom	*n*	*r*	σ^2/*BVS*	*R*
O	1	1.82 (2)	0.004 (2)/2.08	0.003
O	3	2.00 (9)		
NNN shell				
Atom	*n*	*r*	σ^2	
Zn	8	3.08 (1)	0.024 (3)	
Al	4	3.13 (2)		

r; distances (Å), *n*; neighbour numbers, σ^2; distance variances (Debye–Waller factors, Å^2), and BVS; bond valence sum.

Nevertheless, the main structures are well recovered and therefore the fit procedure can be trust with a sensible confidence.

In addition, and more remarkably, the compound which is formed onto the $(11\bar{2}0)_{ZnO}\|(1\bar{1}02)_{sapphire}$ and $(0001)_{ZnO}\|(0001)_{sapphire}$ interfaces *is not* the $ZnAl_2O_4$ spinel, as it is confirmed by a direct comparison of its XAS spectrum with that of a powder sample of $ZnAl_2O_4$. As a matter of fact, preliminary electron diffraction (ED) measurements performed on a cross section of the $(11\bar{2}0)_{ZnO}\|(1\bar{1}02)_{sapphire}$ interface confirmed that this material is highly crystalline. Unfortunately we were able to collect ED data for only one zone axis, showing a diffraction pattern that can be indexed with a centered rectangular lattice having $a \cong 15.3$ Å and $b \cong 4.6$ Å. The HRTEM image and the ED pattern are shown in Fig. 7. In lack of 3-D information, no detailed structural characterization could be obtained, but the results are sufficient to infer that a new mixed Zn/Al oxide, not yet reported in the equilibrium phase diagram, is formed. Moreover, the quite large value of one lattice constant is

Table 2
Same as Table 1, but for the spectrum of Fig. 6.

$(11\bar{2}0)_{ZnO}\|\|(1\bar{1}02)_{sapphire}$, model 1				
NN shell				
Atom	*n*	*R*	σ^2/*BVS*	*R*
Zn–O	1	1.99 (2)	0.010 (4)/1.54	0.030
Zn–O	3	2.079 (7)		
NNN shell				
Atom	*n*	*R*	σ^2	
Zn–Zn	12	3.68 (7)	0.05 (4)	
Zn–Al	0	–		
$(11\bar{2}0)_{ZnO}\|\|(1\bar{1}02)_{sapphire}$, model 2				
NN shell				
Atom	*n*	*R*	σ^2/*BVS*	*R*
Zn–O	1	2.0 (1)	0.01 (4)/1.68	0.01
Zn–O	3	2.0 (8)		
NNN shell				
Atom	*n*	*R*	σ^2	
Zn–Zn	10	3.23 (1)	0.03 (1)	
Zn–Al	2	3.22 (5)		
$(11\bar{2}0)_{ZnO}\|\|(1\bar{1}02)_{sapphire}$, model 3				
NN shell				
Atom	*n*	*R*	σ^2/*BVS*	*R*
Zn–O	1	2.0 (6)	0.01 (2)/1.67	0.008
Zn–O	3	2.0 (1)		
NNN shell				
Atom	*n*	*R*	σ^2	
Zn–Zn	7	3.23 (1)	0.028 (7)	
Zn–Al	5	3.46 (3)		
$(11\bar{2}0)_{ZnO}\|\|(1\bar{1}02)_{sapphire}$, model 4				
NNN shell				
Atom	*n*	*R*	σ^2/*BVS*	*R*
Zn–O	1	1.90 (4)	0.004 (4)/1.80	0.016
Zn–O	3	2.037 (8)		
NNN shell				
Atom	*n*	*R*	σ^2	
Zn–Zn	6	3.077 (8)	0.011 (1)	
Zn–Al	6	3.601 (8)		

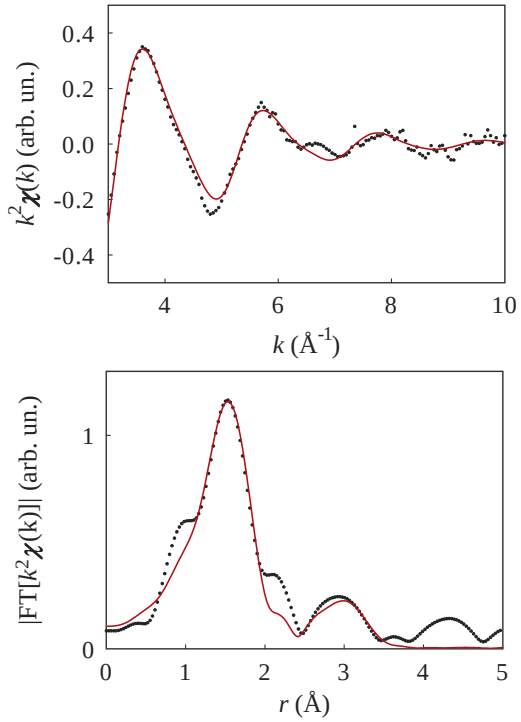

Fig. 6. EXAFS fitting results for the $(11\bar{2}0)_{ZnO}\|(1\bar{1}02)_{sapphire}$ interface at 800 °C, according to model 4 of Table 2 (dots: experimental; line: predicted).

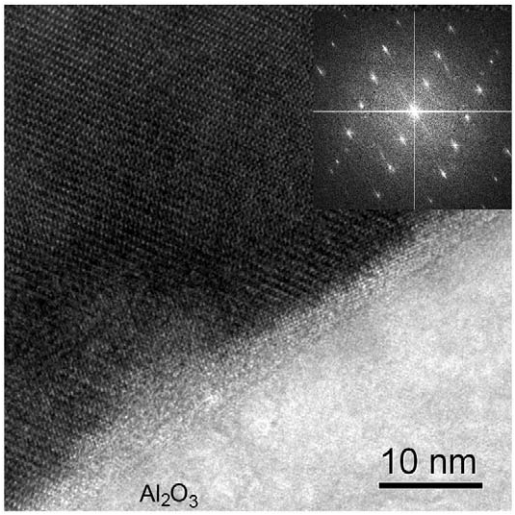

Fig. 7. HRTEM image for the $(11\bar{2}0)_{ZnO}\|(1\bar{1}02)_{sapphire}$ interface at 800 °C. The inset shows an electron diffraction pattern of the reaction product.

reasonably indicative of a non trivial crystal structure. A sound hypothesis is that the interfacial free energy plays a crucial role in stabilizing this new compound. As a final remark, it may be worth to point out that the hypothesis that the $(11\bar{2}0)_{ZnO}\|(1\bar{1}02)_{sapphire}$ and $(0001)_{ZnO}\|(0001)_{sapphire}$ interfaces yield two different compounds should not be discarded on the basis of the EXAFS fit results. A closer inspection of Figs. 5 and 6, indeed, reveals that the spectra are different for what concerns some minor structures (see for example the features near 5 and 7 Å^{-1}), thus supporting the above hypothesis.

Finally, Fig. 8 shows the changes in the film morphology after the treatments at 800 °C, as detected by AFM imaging. The mapped area is $20\times20\,\mu m^2$ in each case. While for the $(11\bar{2}0)_{ZnO}\|(1\bar{1}02)_{sapphire}$ and $(0001)_{ZnO}\|(0001)_{sapphire}$ interfaces the ZnO film collapsed into quite large prismatic twins, for the $(0001)_{ZnO}\|(11\bar{2}0)_{sapphire}$ interface, (the case giving rise to the spinel phase) the final morphology is less altered, with the formation of polycrystalline aggregates with a mean surface roughness of 30 nm. The twins are larger for the $(11\bar{2}0)_{ZnO}\|(1\bar{1}02)_{sapphire}$ interface than for $(0001)_{ZnO}\|(0001)_{sapphire}$ one, and are slightly different in shape. This may give additional endorsement to the previous hypothesis of the formation of two different phases onto these interfaces.

In a previous work by some of the present authors on the NiO–Al_2O_3 system [3], qualitatively similar results (damping of higher metal-metal shells) were interpreted as intermediate formation of a disordered Al-substituted NiO phase as NiO is transformed into $NiAl_2O_4$. Given the idea that the different orientations of the Al_2O_3 substrate present different reactivities of the interfaces, one may think that a similar situation may apply for ZnO–Al_2O_3: the less reactive interfaces are quenched at the stage of the disordered intermediate after treatment at 800 °C, while the most reactive interface has already transformed into spinel with the intermediate remaining undiscovered. This may lead to the conclusion that what is observed here is a purely kinetic effect. However, if this were the case, it would be difficult (if not impossible) to explain the spectacular changes in morphology observed on the interfaces that do not give the spinel. In fact, this change in morphology can be attributed only to

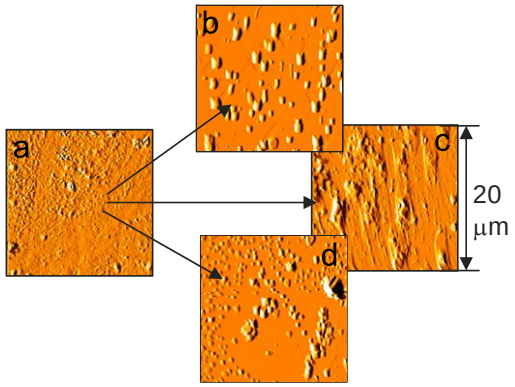

a) Unreacted ZnO film
b) Reacted $(1\ 1\ \bar{2}\ 0)_{ZnO}$ || $(1\bar{1}\ 0\ 2)_{sapphire}$ interface
c) Reacted $(0\ 0\ 0\ 1)_{ZnO}$ || $(1\ 1\ \bar{2}\ 0)_{sapphire}$ interface
d) Reacted $(0\ 0\ 0\ 1)_{ZnO}$ || $(0\ 0\ 0\ 1)_{sapphire}$ interface

Fig. 8. Morphology of some of the investigated samples as detected by AFM imaging.

the different interfacial free energy at the surfaces, and therefore is a thermodynamic effect. This is equivalent to state that different topotactical relationships determine different values for the interfacial free energy and therefore can direct the interfacial reaction towards different products.

4. Conclusions

In conclusion, the present work reports on the reactivity of thin layers (ca. 10 nm thick) of ZnO deposited onto differently oriented Al_2O_3 single crystals. It is found that different chemical processes take place at 800 °C depending on the topotactic relationships between the ZnO film and the Al_2O_3 single crystals: In particular:

(1) Thermal heating at 800 °C causes a spectacular change in the morphology of the $(11\bar{2}0)_{ZnO}\|(1\bar{1}02)_{sapphire}$ and $(0001)_{ZnO}\|(0001)_{sapphire}$ deposited layer, with the formation of prismatic twins.
(2) This change in morphology is caused by a chemical reaction between ZnO and Al_2O_3 to form a Zn/Al mixed oxide, or, possibly two different Zn/Al mixed oxides.
(3) This(these) compound(s) has(have) not yet been reported in the literature. The Zn–O coordination is tetrahedral and strongly resembles that of the wurtzite structure of ZnO. However, some Al is in the NNN shell of Zn.
(4) On the contrary, the $(0001)_{ZnO}\|(11\bar{2}0)_{sapphire}$ interface yields the $ZnAl_2O_4$ spinel and the film remain more stable in its morphology.
(5) The experimental findings demonstrate that XAS spectroscopy can be a useful tool for investigating the early stages of solid-state reactions.
(6) It can also be concluded that in the early stages a solid-state reaction is controlled by the topotactic relationships between the two reacting solids not only for what concerns the kinetics and mechanism, but even the chemical nature of the product.

Further work is planned to clarify the crystal structure of the new compound(s), and to elucidate the range of solubility of Al in this(these) structure(s), with the aim of gaining further light into the mechanisms and kinetics of these processes.

Acknowledgments

The authors acknowledge the European Synchrotron Radiation Facility for provision of beamtime (Experiment CH 2427). The technician H. Pais and the GILDA beamline staff is also acknowledged for considerable help during data collection. GILDA is a project jointly financed by CNR and INFN. Finally, thanks are due to L. Malavasi (University of Pavia) is for helping in sample preparation.

References

[1] H. Schmalzried, Solid State Reactions, Verlag Chemie, Weinheim, 1981.
[2] F. D'Acapito, P. Ghigna, I. Alessandri, A. Cardelli, I. Davoli, Nucl. Instrum. Methods Phys. Res. B 200 (2003) 421–424.
[3] P. Ghigna, G. Spinolo, I. Alessandri, I. Davoli, F. D'Acapito, Phys. Chem. Chem. Phys. 5 (2003) 2244–2247.
[4] E.N. Bunting, Bur. Stand. J. Res. 8 (1932) 280.
[5] S.-H. Lim, D. Shindo, H.-B. Kang, K. Nakamura, J. Cryst. Growth 225 (2001) 202–207.
[6] M. Ay, A. Nefedov, S. Gil Girol, Ch. Wöll, H. Zabel, Thin solid films 510 (2006) 346–350.
[7] F. Raimondi, B. Schnyder, R. Kötz, R. Schelldorfer, T. Jung, J. Wambach, A. Wokaun, Surf. Sci. 532–535 (2003) 383–389.
[8] B. Sang, M. Konagai, Jpn. J. Appl. Phys. 35 (Part 2) (1996) L206–L208.
[9] T.L. Yang, D.H. Zhang, J. Ma, H.L. Ma, Y. Chen, Thin Solid Films 326 (1998) 60–62.
[10] J.R. Neal, A.J. Behan, R.M. Ibrahim, H.J. Blythe, M. Zise, A.M. Fox, G.A. Ghring, Phys. Rev. Lett. 96 (2006) 197–208.
[11] K.B. Sundaram, A. Khan, Thin Solid Films 295 (1996) 87–91.
[12] F. D'Acapito, S. Colonna, S. Pascarelli, G. Antonioli, A. Balerna, A. Bazzini, F. Boscherini, F. Campolungo, G. Chini, G. Dalba, I. Davoli, P. Fornasini, R. Graziola, G. Lichieri, C. Meneghini, F. Rocca, L. Sangiorgio, V. Sciarra, V. Tullio, S. Mobilio, ESRF Newsl. 30 (1998) 42–44.
[13] A.L. Ankudinov, B. Ravel, J.J. Rehr, S.D. Conradson, Phys. Rev. B 58 (1998) 65–75.
[14] T. Mizoguchi, T. Tanaka, S. Yoshioka, M. Kunisu, T. Yamamoto, W.Y. Ching, Phys. Rev. Lett. B 70 (2004) 45–103.
[15] F. D'Acapito, F. Boscherini, S. Mobilio, A. Rizzi, R. Lantier, Phys. Rev. B 66 (2002) 205–411.